Design of acrylated epoxidized soybean oil biobased photo-curable formulations for 3D printing

Design of Acrylated Epoxidized Soybean Oil biobased photo-curable formulations for 3D printing

Matilde Porcarello[1], Cristian Mendes-Felipe[1,2], Senentxu Lanceros-Mendez[2,3], Marco Sangermano[1]

[1] Department of Applied Science and Technology (DISAT), Politecnico di Torino, 10129 Torino, Italy; marco.sangermano@polito.it
[2] BCMaterials, Basque Center for Materials, Applications and Nanostructures, UPV/EHU Science Park, 48940 Leioa, Spain;
[3] IKERBASQUE, Basque Foundation for Science, 48009 Bilbao, Spain.

Corresponding author: Cristian Mendes-Felipe (cristian.mendes@bcmaterials.net)

Abstract

In recent decades, the significance of developing polymeric materials derived from renewable bio-based sources has grown due to the pressing environmental concerns facing our planet. Moreover, the diminishing availability of oil, the primary carbon resource for polymer production, led to the research of alternative sources with low environmental impact. From this perspective, vegetable oils (VO) have emerged as an interesting option due to their abundant presence and cost-effectiveness, along with the presence of numerous reactive groups. Among these, soybean oil stands out as one of the most widely used options, thanks to its potential for functionalization through epoxidation and subsequent acrylation, resulting in acrylate epoxidized soybean oil (AESO). In this study AESO was employed as a primary raw material for Digital Light Processing (DLP) because of its photocurable nature. Because of its high viscosity, four monofunctional reactive diluents, namely lauryl acrylate (LA), lauryl methacrylate (LMA), isobornyl acrylate (IBOA) and isorbornyl methacrylate (IBOMA), were incorporated in different weight percentages. Reactivity and rheological properties of these formulations were investigated. Subsequently, formulations with viscosities suitable for the DLP process were employed to 3D print objects. These printed samples were then subjected to mechanical and thermo-mechanical analyses. Moreover, more complex shaped objects were printed to evaluate the precision of the printing process using these formulations.

Keywords

Biobased, photocurable, soybean oil, acrylic, 3D printing.

1. Introduction

Additive manufacturing (AM) is developing a key role as an innovative production method. In fact, it represents a technology that has revolutionized the area of manufacturing. Traditional methods are mainly subtractive, involving cutting or shaping materials, leading to large materials waste and energy use. AM, on the other hand, is focused on building objects in a layer-by-layer manner, by adding material only where needed. Together with the reduction of waste, there are several further advantages like versatility, accuracy, rapid prototyping, and reduced or no post processing needs [1]. AM relies on different techniques that enable to process a large variety of materials like polymers, metals, ceramic materials, and composites. This has allowed developments of components in various fields like aerospace, food [2] and construction sector [3], but also in the biomedical industry [4,5]. Further, it has been proven that AM may have a very important effect on sustainable production, contributing to the development of green solutions, lowering the excessive use of limited resources [6]. A significant category of AM is represented by VAT polymerization (VP). It is a set of techniques characterized by the fabrication of 3D objects from liquid resins which are photocured by a light source. Inside the vat is placed the photopolymer in the form of monomers and oligomers mixed with the photoinitiator, a species capable of absorbing light radiation. When the photoinitiator is exposed to light (UV or visible), it triggers the reaction by interacting with the monomers and oligomers generating longer chains [7]. Therefore, the photoinitiator must be selected according to the wavelength of the light source. VP offers many advantages in terms of accuracy, because of its ability to print detailed objects with high resolution [8]. In terms of precision, Digital Light Processing (DLP), one of the most used VP methods, can produce high-resolution patterns. It shows also other advantages like its speed, cost-effectiveness, and ability to work at room temperature [9]. From the material point of view, it is essential to design photocurable formulations showing reactivity towards photopolymerization and adequate viscosity. This latter characteristic must be low enough to allow the resin to flow within the printing area, since in VAT polymerization techniques no device is provided for mechanically distributing the material. To reduce the viscosity value, it is possible to use reactive diluents [10], which will participate in the crosslinking reaction forming the cured polymeric network.

Up to now, VP is characterized by a limited choice of bio-based photopolymerizable resins [11], commercially available photopolymers for VP being mainly acrylates or epoxides from fossil fuel sources. Considering both the environmental impact and limited availability of fossil resources, it is essential to replace resins from oil with bio-based alternatives, in order to support the transition towards a more sustainable and circular economy. Among the possible alternatives, those that have aroused the greatest interest are vegetable oils (VOs), because they are abundant, inexpensive, and attractive from the point of view of their structure [12]. Indeed, the carbon-carbon double bonds in their molecular chains make them able to be chemically modified by epoxidation and/or acrylation reactions to be processed by photopolymerization [13]. VOs rarely contain functional groups, like Vernonia oil, in which epoxy groups are present [14]. There is a large variety of VOs potentially suitable for VP like modified linseed oil [7],

castor oil [15], and cardanol oil [16], since they exhibit UV curable properties [17]. Recent studies proved that also canola and sunflower oil after acrylation can be promising as DLP inks [16]. At the present moment, however, the most relevant oil for 3D printing is soybean oil. Among VOs, it is one of the most globally produced and it is characterized by biocompatibility, biodegradability, and high functionalization capability thanks to its reactive unsaturated double bonds [18]. Indeed, it was one of the first modified VOs used in AM as ink, for bio scaffolds development through stereolithography (SLA) 3D printing [19]. Acrylated epoxidized soybean oil (AESO) can be easily and rapidly polymerized by free radical reaction thanks to the presence of acrylated groups, which make this variant of soybean oil interesting for VP technologies [20]. However, 3D printing of pure AESO is challenging and time consuming, due to its high viscosity [18]. As mentioned before, reactive diluents can be added to control AESO viscosity, like isobornyl (meth)acrylate [18,21] and eugenol-based methacrylate [22], among others.

In this context, the aim of this work is to produce and characterize formulations containing AESO mixed with different reactive diluents, including lauryl acrylate (LA), lauryl methacrylate (LMA), isobornyl acrylate (LA), and isobornyl methacrylate (IBOMA) as suitable supply materials for DLP 3D printing. Those formulations will be optimized to obtain printed objects with high resolution and refinement, and it will be determined whether those biobased formulations can be competitive with commercial resins. For this purpose, complex shaped objects are printed and analyzed by the evaluation of the mechanical and thermo-mechanical properties.

2. Materials and Methods

2.1. Materials

Acrylated epoxidized soybean oil, with density of 1.04 g/mL at 25°C was purchased from Sigma-Aldrich (Milano, Italy). Reactive diluents lauryl acrylate (with density of 0.884 g/mL at 25 °C), lauryl methacrylate (with density of 0.868 g/mL at 25°C), isobornyl acrylate (with density of 0.986 g/mL at 25°C) and isobornyl methacrylate (with density of 0.983 g/mL at 25°C) were also purchased from Sigma-Aldrich (Milano, Italy). Photoinitiator Irgacure 819 (BAPO) was purchased from Ciba (Basilea, Switzerland). The isopropanol used for cleaning was purchased by Sigma-Aldrich (Milano, Italy), purity 99.5 % and density of 0.785 g/mL at 25 °C.

2.2. Formulation and 3D printing Process

Four different reactive diluents were added to AESO monomer in weight percentages from 0 % to 50 %. In each formulation 1 phr of Irgacure 819 was added. Further information about the nomenclature of the formulations is shown in Table 1.

Table 1. *Information about nomenclature and weight percentages of the formulations prepared.*

Name	Weight percentage of AESO (%wt.)	Weight percentage of reactive diluent (%wt.)
100-0	100	0
90-10	90	10
80-20	80	20
70-30	70	30
60-40	60	40
50-50	50	50

The components were mixed using a heating magnetic stirrer (by Velp Scientifica) at 100 °C and 500 rpm, for 90 minutes. Subsequently, an ultrasonic bath (by Orma Scientific Instruments) was used. The samples for dynamic mechanical thermal analysis (DMTA), tensile analysis, 3D scanner and optical microscope analyses were printed using a digital light processing (DLP) printer, Asiga MAX UVX27 (Asiga, Australia) equipped with a LED light source of 385 nm (XY pixel resolution is 27 µm while Z-axis resolution is 1-500 µm). Every printed layer had a thickness of 50 µm and as irradiated for 1 s with a light intensity of 38 mW/cm^2. Separation rate and separation distance parameters were modified according to the formulation used and the ranges were respectively 1.5-2.475 mm/s and 10-18 mm. After printing, every sample was washed in isopropanol and inserted into ultrasonic bath for 5 minutes. Then the post curing process was performed for 3 minutes at 10 mW/cm^2 with a Asiga Flash Cure UV lamp (Asiga, Australia).

2.3. Characterization techniques

2.3.1. Photo-rheology and viscosity

Photo-rheological and viscosity measurements were performed using an Anton PAAR Modular Compact Rheometer (Physica MCR 302, Graz, Austria) in plate-plate geometry with plates measuring 25 mm in diameter. During photo-rheology analysis a Hamamatsu LC8 lamp was used as source of light (15 mW/cm^2) which was positioned under the bottom plate and activated after 60 s from the start of each test. For this analysis, the bottom plate was substituted by a glass one, and the separation gap between the plates was 0.3 mm. The shear frequency was kept constant at 1 Hz. With this kind of analysis, it was possible to investigate the UV-curing process of the formulations. Viscosity was estimated in a range of shear rate from 0.01 and 1000 s^{-1} using a separation gap between the plates of 1 mm. All the measurements were performed at room temperature and in triplicate for each sample.

2.3.2. Dynamic mechanical thermal analysis (DMTA)

Thermo-mechanical analysis was performed using a Triton Technology instrument model Tritec 2000 in tension mode. During the tests, a uniaxial stress with 1 Hz of frequency was applied. The starting temperature of -60 °C was achieved using liquid nitrogen. Then the sample was heated at a rate of 3 °C/min until rubbery plateau was reached. This kind of analysis was used to determine the glass transition temperature, which corresponds to the peak of tan δ vs temperature curve. Also, the crosslinking density (ν_c) was evaluated through Eq. 1.

$$\nu_C = \frac{E'}{3RT} \quad , \tag{1}$$

where ν_c is the number of crosslinks per volume of the crosslinked network, E' is the storage modulus in the rubbery plateau registered at temperature T = T_g + 50 °C, expressed in Kelvin and R is the gas constant.

The samples used in this analysis were 3D printed as reported in 2.2 with average dimension of 0.5 x 3.5 x 13 mm.

2.3.3. Tensile mechanical measurements

Mechanical properties were analyzed using a MTS QTestTM/10 Elite (MTS System Corporation, Eden Prairie, MN, USA) instrument. The samples used during the analysis were dog bone shaped and 3D printed as explained in 2.2 with average dimension of 2 x 5 x 50 mm^3. A 500 N load cell was used and the tensile stress was applied with a speed of 5 mm/min. From each test, a stress-strain curve was obtained. From these curves it was possible to obtain the value of Young's modulus (E), calculated as the tangent of the curve in the linear area, and the maximum strain value. Each trial ended with the breaking of the sample. The modulus and ultimate strain values were the result of the average of the three samples analyzed for each formulation.

2.3.4. 3D Scan Imaging

The purpose of the 3D Scanner analysis was to investigate the reliability of DLP printing process with the formulations prepared on complex shaped objects. For these measurements it was used an instrument from 3Shape company (Copenhagen, Denmark) model E4 3D with an accuracy of 4 µm. Through the software, a comparison was carried out by an overlay between the digital file and a scan of the printed object. The software returned a heat map showing less precise areas in red, thus reporting potential errors during the printing process. The objects were covered with talcum powder to improve scanning performance during the test.

2.3.5. Optical microscopy

Precision and accuracy measurements of the 3D printing process was carried out using Laborlux 12 ME S optical microscope from Leitz. Thickness evaluations were estimated with this instrument, comparing the

results with the theoretical values of thickness of the STL files. In this way, it was possible to determine the error attributed to the printing process with the developed formulations.

3. Results and Discussion

3.1. Characterization of liquid formulations and 3D-printing

The UV-curing process was investigated through photo rheology analysis, to determine the influence of the reactive diluents on the reactivity of the formulations. Two parameters were calculated, the curing rate, which corresponds to the slope of the curve storage modulus (G') vs time, and the gelification time (t_{gel}), that occurs when G' is equal to the loss modulus (G'') [23]. In Fig. 1 the G' vs time is presented for the AESO-based formulations containing LA as reactive diluent.

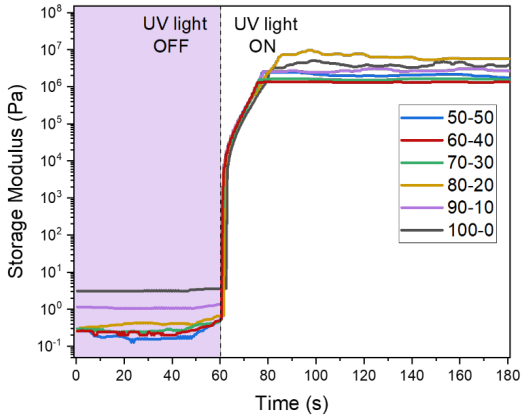

Fig. 1. *Photorheology curves for AESO-LA formulations.*

Fig. 1 shows that when the light is off, the modulus G' is constant and low for all formulations. After 60 s, the light is switched on and G' rapidly increases in several order of magnitude due to the crosslinking reaction until reaching a constant value. Since a similar behavior is also observed in the formulations containing LMA, IBOA and IBOMA., only the photorheological curves of AESO-LA formulations are reported. On the other hand, different values of curing rate and t_{gel} were observed, depending on the type of reactive diluent and the amount employed. These data are shown Fig. 2 for the different formulations.

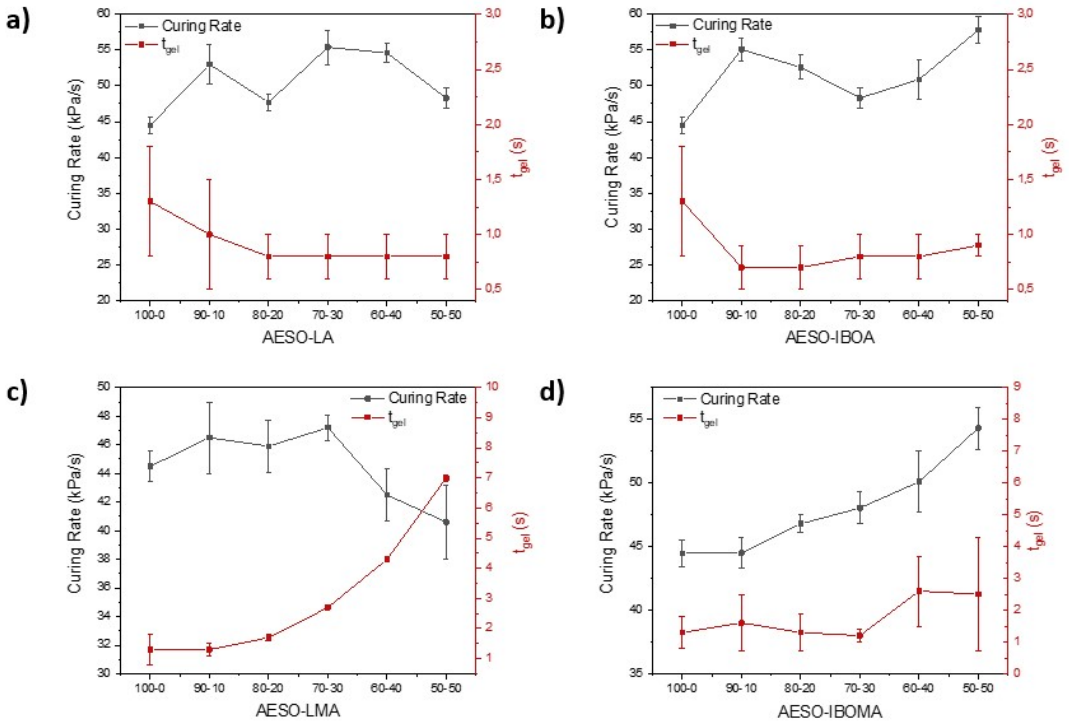

Fig. 2. *Curing rate and t_{gel} trends for AESO-based formulations containing different reactive diluents:* ***(a)*** *LA,* ***(b)*** *IBOA,* ***(c)*** *LMA,* ***(d)*** *IBOMA.*

Formulations containing acrylate reactive diluents (Fig. 2a and Fig. 2b) showed a slight increase of curing rate values in comparison to pristine AESO. On the other hand, there is a decrease in t_{gel} values with respect to the pristine AESO formulation. Both these trends can be explained through a lowering of viscosity, which implies an incensement in chains mobility [24]. Therefore, even if LA and IBOA show two different chemical structures, they act in the same way in terms of photoreactivity of the formulations.

Methacrylate reactive diluents (Fig. 2c and Fig. 2d) exhibit a different behavior. Curing rate values can be considered constant for formulations with LMA, while there is a slight increase of this parameter in formulations with IBOMA. In both cases, t_{gel} values increase with the addition of the reactive diluent. This effect is attributed to a lower reactivity of methacrylic groups in comparison to the acrylic ones [25], which is more evident in formulations containing LMA.

As previously mentioned, reactive diluents were added with the purpose of decreasing the viscosity of the photocurable formulations to make them suitable for 3D printing. In Fig. 3 the viscosity vs shear rate curves of the formulations with AESO and LA are shown as a representative example. From the graph, it is possible to state that the formulations present overall a Newtonian behavior (constant viscosity as the shear rate increases) [24] in the considered shear rate range.

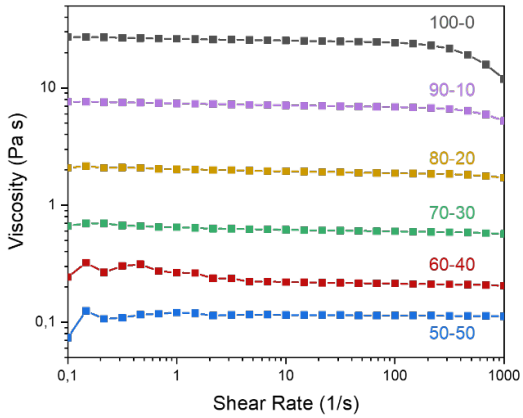

Fig. 3. *Viscosity as function of shear rate for the photocurable formulation AESO-LA.*

At high shear rate values, the viscosity starts to decrease, in particular for the formulations with high weight percentages of AESO. This trend is visible also in the formulations with the other reactive diluents used in this work. The viscosity measured at 1 s^{-1} was selected as the reference value to compare the effects on viscosity of the photocurable formulations of the different reactive diluents. The corresponding data are collected in Table 2.

Table 2. *Viscosity values (Pa s) registered at 1 s^{-1} for the different AESO-based formulations.*

Formulation (AESO-react. dil.) %wt.	**Viscosity at 1 s^{-1} (Pa s)**			
	LA	**IBOA**	**LMA**	**IBOMA**
100-0	25.2 ± 1.4			
90-10	7.29 ± 0.28	10.5 ± 0.2	6.49 ± 0.46	7.76 ± 0.03
80-20	2.00 ± 0.04	4.07 ± 0.05	2.06 ± 0.03	3.21 ± 0.07
70-30	0.62 ± 0.06	1.72 ± 0.05	0.69 ± 0.03	1.43 ± 0.04
60-40	0.26 ± 0.01	0.66 ± 0.01	0.27 ± 0.01	0.56 ± 0.01
50-50	0.12 ± 0.01	0.29 ± 0.01	0.10 ± 0.02	0.28 ± 0.01

Table 2 shows that LA and LMA present a higher influence on viscosity than IBOA and IBOMA, which is related to the different density of the diluents and as can be seen in the experimental section of the present work. LA and LMA are characterized by a similar density value and lower than the ones of IBOA and IBOMA. This involves adding a greater volume of LA and LMA for the same weight, compared to the IBOA and IBOMA, leading, therefore, to lower viscosities for the LA and LMA formulations.

After rheological analyses, some preliminary 3D printing tests were carried out to determine whether the formulations were suitable for DLP printing and to define the optimal parameters of the process. As explained before, pristine AESO has too high viscosity for 3D-printing applications. Formulations with 10 %wt. of diluent are also not printable because of their high viscosity. Formulations with 20 %wt. of reactive diluent are printable but using specific printing conditions. In particular, two parameters were modified as

anticipated in paragraph 2.2, separation rate which was decreased from 2.475 to 1.5 m/s and separation distance which was increased from 10 to 18 mm. These changes were carried out to give the platform more time to collect resin from the vat and avoid holes in the printed object. The remaining formulations were processed using the parameters discussed before.

3.2. Characterizations of the printed samples

3.2.1. Thermo-mechanical properties

DMTA tests were performed to analyze thermo-mechanical properties of the printed samples with AESO and reactive diluents. From the graphs obtained it was possible to determine the T_g and the storage modulus E'. Fig. 4 shows the curves of tan(δ) and E' vs temperature for AESO-IBOMA printed samples. The results were compared to a sample consisting of 100% AESO, obtained by casting in a mold of the same dimensions as the printed samples and subsequent cross-linking with a DYMAX UV lamp at 130 mW/cm^2 for 30 s.

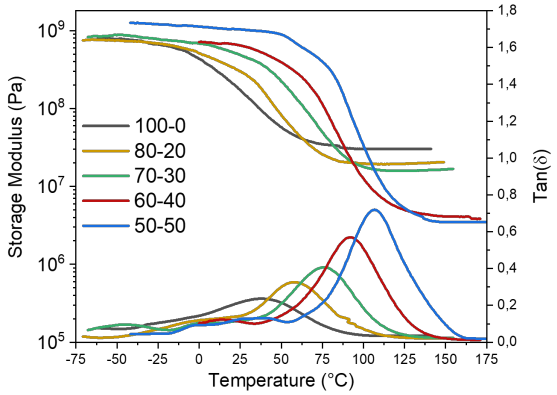

Fig. 4. *DMTA results for AESO-IBOMA printed specimens.*

Using Eq. 1 (Section 2.3.2) ν_c was calculated. The values of T_g, E' and ν_c are shown in Table 3 and Table 4.

Table 3. *Thermo-mechanical properties evaluated by DMTA for AESO-LA and AESO-IBOA samples.*

Formulation (AESO-react. dil.) %wt.	**LA**			**IBOA**		
	T_g (°C)	*E' (kPa)*	*ν_c (mmol/L)*	*T_g (°C)*	*E' (kPa)*	*ν_c (mmol/L)*
100-0	38	31174	3460	38	31174	3460
80-20	20	25300	2960	47	20377	2210
70-30	18	17440	2050	49	17517	1890
60-40	9	16114	1950	56	13600	1440
50-50	-5	9405	1190	59	11440	1200

Table 4. *Thermo-mechanical properties evaluated by DMTA for AESO-LMA and AESO-IBOMA samples.*

Formulation	**LMA**	**IBOMA**

(AESO-react. dil.) %wt.	T_g (°C)	E' (kPa)	ν_c (mmol/L)	T_g (°C)	E' (kPa)	ν_c (mmol/L)
100-0	38	31174	3460	38	31174	3460
80-20	34	25164	2830	58	19319	2030
70-30	29	17451	1990	76	15805	1590
60-40	25	6336	730	92	4232	410
50-50	18	137	20	107	3462	30

In the case of formulations with LA and LMA, the addition of reactive diluents caused a lowering of the T_g. Instead, formulations with IBOA and IBOMA showed an opposite effect on T_g values. This phenomenon can be explained by considering two variables: the crosslinking density ν_c and the structure of the added reactive diluent. From the ν_c values shown in Table 3 and Table 4 it is observed how the addition of the diluent induced a decrease of the cross-linking density in comparison to AESO. This is because monofunctional reactive diluents cannot form interchain links and induced a decrease of the crosslinking density of the polymeric network Consequently, glass transition temperature of photo-crosslinked polymers will be lower [26]. However, reactive diluents are characterized by different chemical structures. LA and LMA show a linear structure, while IBOA and IBOMA show a ring in their chemical structures which gives them higher rigidity [27]. For this reason, the addition of IBOA/IBOMA causes a stiffening of the final structure of the polymers with a consequent increase in the T_g, notwithstanding the decrease of the crosslinking density. This means that the contribution to the stiffening of the polymeric lattice attributable to the chemical structure of the monomer is more important than the flexibilization effect due to the lowering of the crosslinking density. This effect is also reflected in the value of the rubbery modulus. In fact, for each resin/diluent system, E' is lower than that of the pristine resin and decreases as the diluent concentration increases.

3.2.2. Tensile properties

Mechanical properties have been investigated through tensile measurements. Fig 5. shows the stress-strain curves of the 3D-printed AESO-based formulations containing the different investigated reactive diluents.

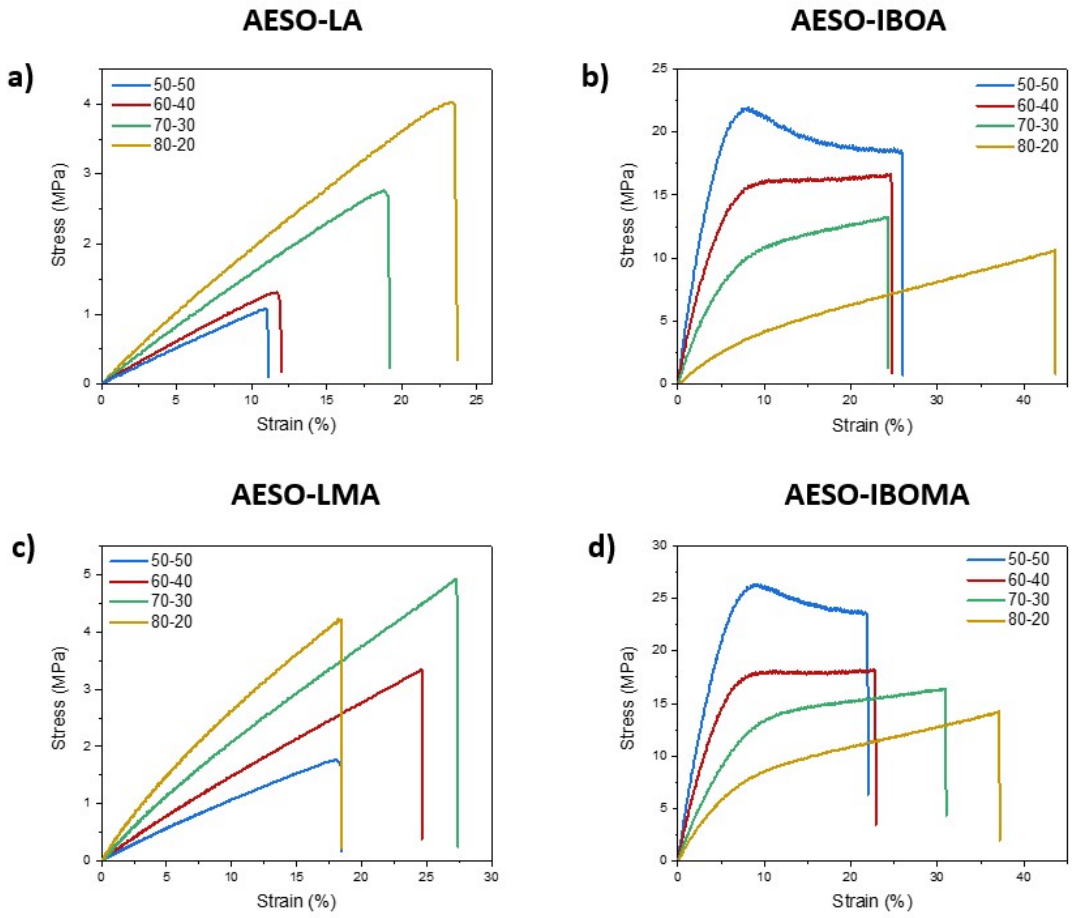

Fig. 5. *Stress-strain curves of 3D printed specimens for AESO-LA (a), AESO-IBOA (b), AESO-LMA (c) and AESO-IBOMA (d) formulations.*

In Table 5 and 6 the values of Young's Modulus and strain at break for all the samples are summarized and compared with the ones of pristine AESO UV-Cured in the mold.

Table 5. *Mechanical properties evaluated by tensile measurements for AESO-LA and AESO-IBOA samples.*

Formulation (AESO-react. dil.) %wt.	**LA**		**IBOA**	
	E (MPa)	*Strain at break (mm/mm)*	*E (MPa)*	*Strain at break (mm/mm)*
100-0	101.9 ± 7.1	0.114 ± 0.017	101.9 ± 7.1	0.114 ± 0.017
80-20	21.8 ± 0.5	0.231 ± 0.029	50.4 ± 8.6	0.446 ± 0.034
70-30	17.3 ± 0.4	0.187 ± 0.039	212.1 ± 16.1	0.223 ± 0.017
60-40	12.9 ± 0.3	0.122 ± 0.012	363.9 ± 11.3	0.231 ± 0.014
50-50	10.0 ± 0.7	0.098 ± 0.023	508.3 ± 17.4	0.080 ± 0.002

Table 6. *Mechanical properties evaluated by tensile measurements for AESO-LMA and AESO-IBOMA samples.*

Formulation (AESO-react. dil.) %wt.	**LMA**		**IBOMA**	
	E (MPa)	*Strain at break (mm/mm)*	*E (MPa)*	*Strain at break (mm/mm)*

100-0	101.9 ± 7.1	0.114 ± 0.017	101.9 ± 7.1	0.114 ± 0.017
80-20	32.1 ± 2.5	0.171 ± 0.046	140.9 ±3.5	0.356 ± 0.043
70-30	23.9 ± 0.3	0.253 ± 0.020	234.1 ± 8.7	0.314 ± 0.043
60-40	17.3 ± 2.0	0.205 ± 0.043	435.2 ± 45.0	0.241 ± 0.146
50-50	12.5 ± 0.2	0.177 ± 0.014	531.4 ± 20.0	0.093 ± 0.005

Considering the stress-strain mechanical curves of formulations with LA and LMA (Fig. 5a and Fig.5c) it is observed that they present just the elastic linear section, and that failure occurs for low strain levels. The values of Young's modulus and strain at break decrease as the content of reactive diluent increases. This effect is related to the decrease of the cross-linking density by increasing the reactive monofunctional diluent in the photocurable formulation. In fact, as previously discussed, the cross-linking density decreases as the amount of reactive diluent increases, lowering the mechanical properties of the 3D-printed samples [28].

The samples containing IBOA/IBOMA as reactive diluent (Fig. 5b and Fig. 5d), on the other hand, also exhibit a plastic regime: the stress-strain curves being characterized by the typical trend of plastic materials, with an extended linear section (elastic region) and a subsequent zone of plastic deformation. Unlike formulations with LA/LMA, the modulus increases with increasing the amount of diluent in the photocurable formulation. As previously explained, this behavior is attributable to the different chemical structure of the two diluents. In fact, the rigid rings inside the structure of IBOA and IBOMA hinder the mobility of the AESO chains [29]. Therefore, overall, these samples are soft, but resistant [30].

3.3. Characterization of the 3D-printing process

Some considerations were made before proceeding with the printing and characterization of more complex objects. First, printing tests were carried out to verify the printability of the selected shapes with the developed formulations. The results showed that the formulations containing the methacrylate reactive diluents had some printing issues, especially in the fabrication of elaborate structures requiring longer processing times (according to photorheological analyses). For these reasons, complex structures were printed just with AESO-LA and AESO-IBOA formulations and then characterized by 3D scanner and optical microscopy.

Accuracy and precision of the process were investigated by printing three objects with different characteristics. STL file images of the samples with theoretical dimensions are shown in Fig. 6. The cube and the gyroid were analyzed through a 3D scanner while the wall system was examined through an optical microscope.

The shapes selected for the characterization of the printing process were chosen because each of them showed different characteristics that can cause issues during 3D printing. The cube contains many open areas, and the structure is very thin and fragile, so the precision of the formulations used in the printing process should be very high to avoid imperfections. The gyroid is made of curved walls whit small open

areas inside, which can trap some resin if it is not adequate for printing. The wall system was chosen because it contains walls with fixed thickness so if the formulation is not suitable for printing, the thickness values measured on the printed object will be very different from the theoretical ones.

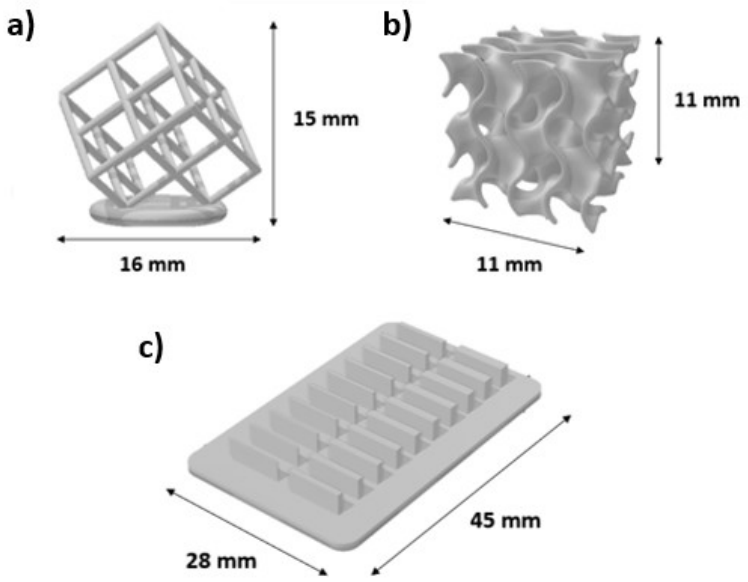

Fig. 6. *CAD project images of printed samples a) hollow cube, b) gyroid and c) wall system.*

3.3.1. 3D Scanner

The analysis with the 3D scanner was conducted to identify the dimensional differences between the printed object and the corresponding STL file, used for the printing process. In Fig. 7 and Fig. 8 are shown the images of cube and gyroid for AESO-LA and AESO-IBOA formulations.

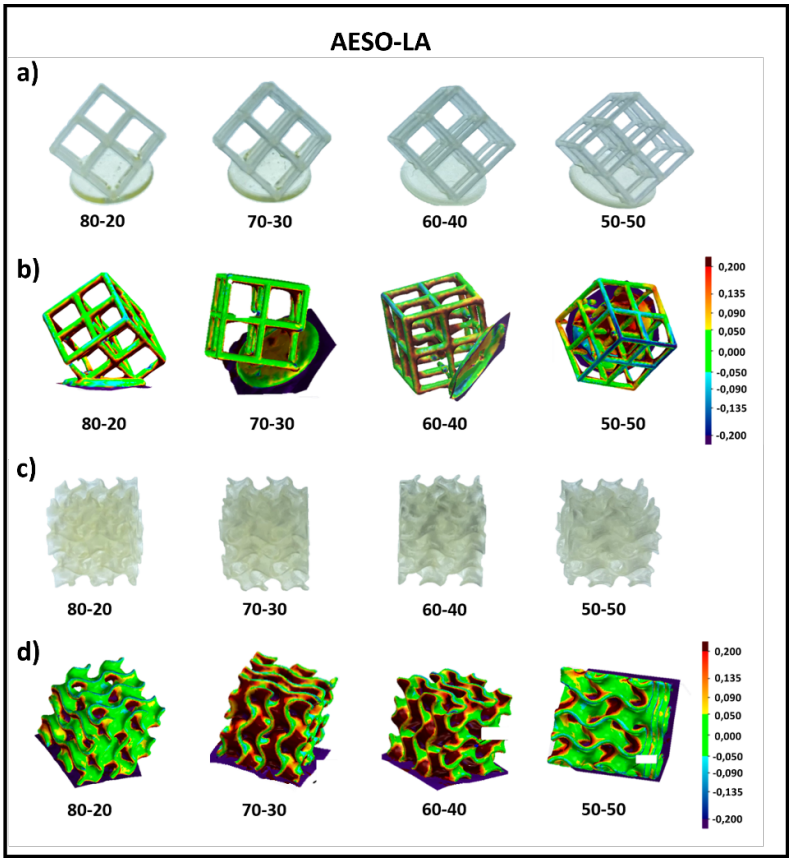

Fig. 7. *Pictures of 3D printed cubes (a) and gyroids (c), compared to their 3D scanner evaluation images of the differences between the CAD project and the real printed object (b) and (d) respectively, for AESO-LA formulations.*

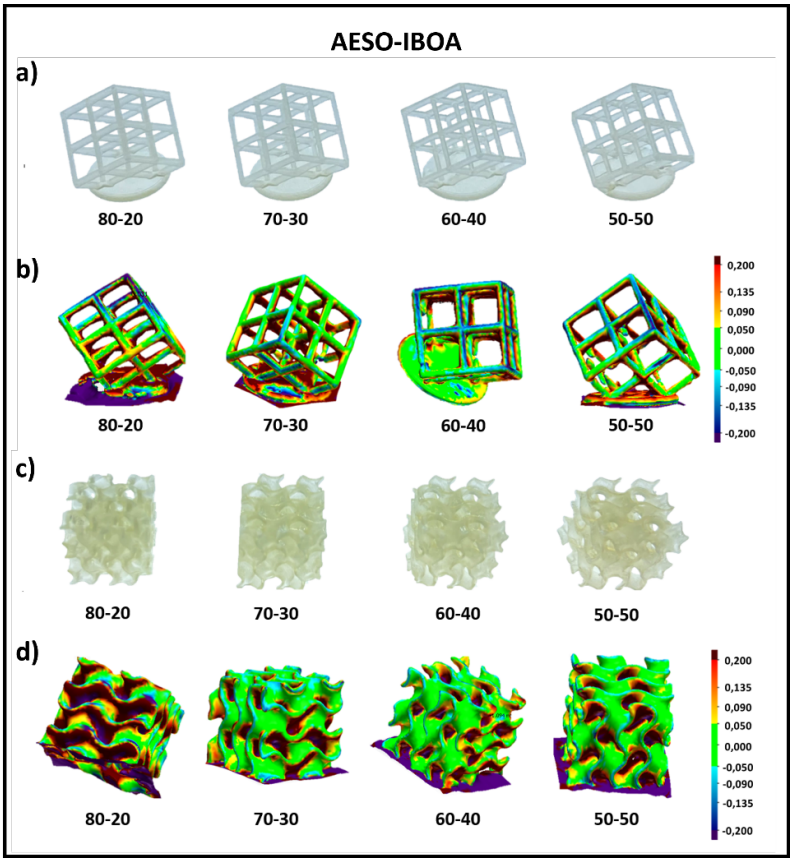

Fig. 8. *Pictures of 3D printed cubes (a) and gyroids (c), compared to their corresponding 3D scanner evaluation images of the differences between the CAD project and the real printed object (b) and (d) respectively, for AESO-IBOA formulations.*

The scanner software also returned the error values calculated as the average of all the points considered by the instrument, with respect to the digital file of the object. These values are represented in Table 7 for both formulations.

Table 7. *Average error on dimensions evaluated through scanner 3D program for AESO-LA and AESO-IBOA printed objects.*

Formulation (AESO-react. dil.) %wt.	**LA**		**IBOA**	
	Average error CUBE	*Average error GYROID*	*Average error CUBE*	*Average error GYROID*
80-20	0,059	0,014	0,066	0,039
70-30	0,067	0,049	0,128	0,047
60-40	0,032	0,055	0,054	0,059
50-50	0,071	0,068	0,052	0,012

The images returned by the 3D scan show different colors: the red areas indicate areas in which the real object is larger than the theoretical one, the blue areas those where the real object has smaller dimensions than the theoretical one, the green areas indicate the areas in which the two are equal. To determine these areas, a tolerance level suitable for the dimensions of the printed object was entered, which for the analysis carried out is ± 0.05. Another variable of this analysis is the amount of talcum powder adhered to the walls

of the objects. In fact, some areas of the cube and all the internal areas of the gyroid, were difficult to reach by the dust. Indeed, it is possible to observe from the images presented in Figures 7 and 8 how most of the red areas are located right inside the objects. This factor certainly influenced the results of the analyzes carried out with this instrument. Errors are small for both formulations in either printed object. In fact, the closer the error value is to zero, the more the real object corresponds to the theoretical one. The quantity of talcum powder adhered to the walls must also be considered in the error analysis. Therefore, it is possible to state, considering both the images and the error value, that the DLP printing accuracy with these formulations is good.

3.3.2. Optical microscopy

The accuracy of the printing method of the system of walls was determined by optical microscopy, by measuring the thickness of 3 walls of the printed object and by comparing with the theoretical value. The walls selected for the measurement are the second of the first row, the first wall of the second row and the eighth wall of the second row, as indicated in Fig. 9.

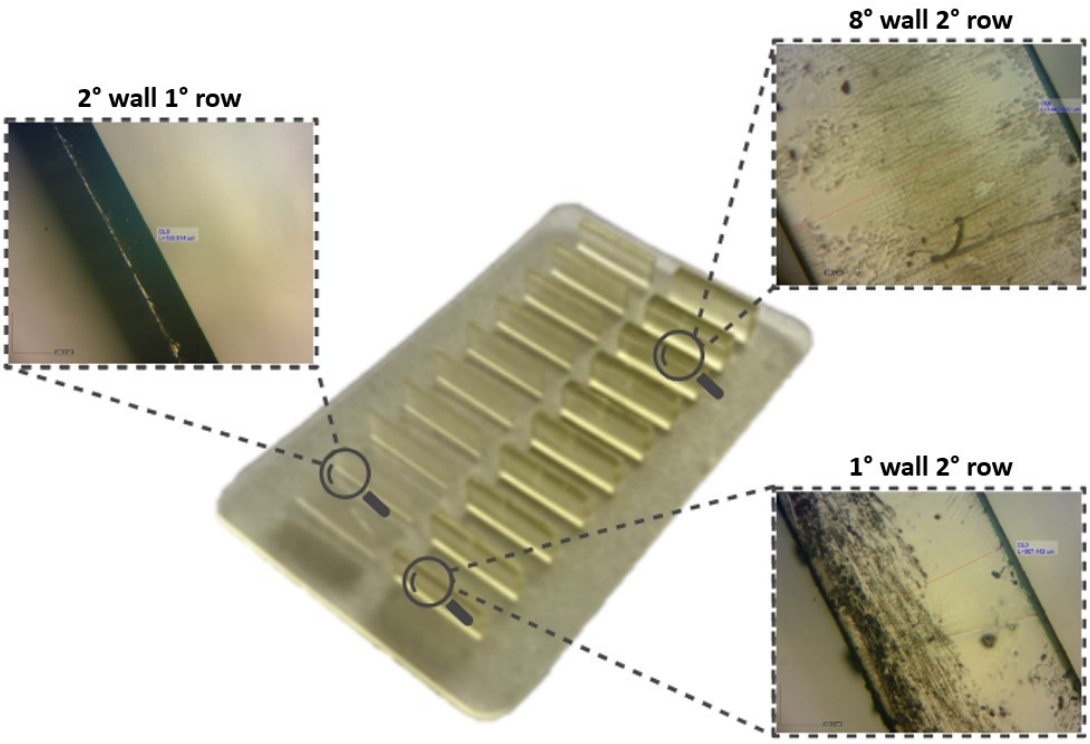

Fig. 9. *3D printed system of walls with magnifications of the selected walls by optical microscope.*

Thickness measurements of the selected walls are presented in Table 8.

Table 8. *Thickness measurements evaluated by optical microscopy for AESO-LA and AESO-IBOA printed objects.*

Formulation (AESO -react. dil.) %wt.	**LA**	**IBOA**
	Thickness (μm)	*Thickness (μm)*

	2° wall 1° row	1° wall 2° row	8° wall 2° row	2° wall 1° row	1° wall 2° row	8° wall 2° row
80-20	167	892	1440	147	889	1440
70-30	170	907	1441	151	863	1441
60-40	158	891	1437	162	889	1444
50-50	-	880	1445	147	889	1432
theoretical	160 ± 27	880 ± 27	1440 ± 27	160 ± 27	880 ± 27	1440 ± 27

As shown in Table 8, all three walls measured for each printed formulation have similar thicknesses and, in some cases, they are equal to the theoretical values. In the case of the formulation AESO-LA(50-50) it was not possible to measure the second wall of the first row as it was very thin and fragile. In general, it can be stated that 3D printing of these structures with the AESO-LA and AESO-IBOA formulations is characterized by a good accuracy.

4. Conclusions

Biobased photocurable formulations were prepared containing acrylated epoxidized soybean oil (AESO) mixed with four monofunctional reactive diluents in different weight percentages. The aim of the work was the investigation of the effect of monofunctional reactive diluents to be used to control the viscosity of the photocurable formulations to make them printable. Rheological and photo-rheological behavior have been investigated to determine whether the viscosity and the reactivity of the formulations were suitable for Digital Light Processing (DLP) 3D printing. In addition, printing tests were carried out establishing that only formulations with 20-50%wt. content of reactive diluent can be processed. Thermomechanical investigation of printed samples showed an increase in glass transition temperature (T_g) when isobornyl acrylate (IBOA) and methacrylate (IBOMA) were added and an opposite trend in specimens with lauryl acrylate (LA) and methacrylate (LMA). This phenomenon was ascribed to the different chemical structures of reactive diluents, therefore to a higher stiffness conferred by IBOA/IBOMA, also confirmed by tensile measurements. Accuracy and precision of the DLP printing process were evaluated through 3D scanner and optical microscopy analyses of complex shaped objects, including hollow cube, gyroid and a wall system. The results demonstrate good reliability of the printing process for objects fabricated with the AESO-LA and AESO-IBOA formulations. In conclusion, this work demonstrates the development of new 3D printing formulations from bio-renewable sources as possible alternatives of commercial fossil-based resins, towards sustainable additive manufacturing solutions.

Acknowledgments

This study forms part of the Advanced Materials program and was supported by MCIN with funding from European Union NextGenerationEU (PRTR-C17.I1) and by the Basque Government under the IKUR program and though the POSTDOC fellowship program (POS-E_2021_2_0001). Funding from the Basque Government Industry Department under the ELKARTEK program is also acknowledged. This study was

partially carried out within the Agritech National Research Center and received funding from the European Union Next-GenerationEU (PIANO NAZIONALE DI RIPRESA E RESILIENZA (PNRR)—MISSIONE 4 COMPONENTE 2, INVESTIMENTO 1.4—D.D.1032 17/06/2022, CN00000022).

References

[1] T.D. Ngo, A. Kashani, G. Imbalzano, K.T.Q. Nguyen, D. Hui, Additive manufacturing (3D printing): A review of materials, methods, applications and challenges, Compos. Part B Eng. 143 (2018) 172–196. https://doi.org/10.1016/j.compositesb.2018.02.012.

[2] J. Lee, A 3d food printing process for the new normal era: A review, Processes. 9 (2021). https://doi.org/10.3390/pr9091495.

[3] C. Buchanan, L. Gardner, Metal 3D printing in construction: A review of methods, research, applications, opportunities and challenges, Eng. Struct. 180 (2019) 332–348. https://doi.org/10.1016/j.engstruct.2018.11.045.

[4] B. Utela, D. Storti, R. Anderson, M. Ganter, A review of process development steps for new material systems in three dimensional printing (3DP), J. Manuf. Process. 10 (2008) 96–104. https://doi.org/10.1016/j.jmapro.2009.03.002.

[5] I. Gibson, D. Rosen, B. Stucker, Additive manufacturing technologies: 3D printing, rapid prototyping, and direct digital manufacturing, second edition, Johnson Matthey Technol. Rev. 59 (2015) 193–198. https://doi.org/10.1007/978-1-4939-2113-3.

[6] M. Ozguner, Z. Ozguner, Evaluation of the importance of additive manufacturing technology in terms of sustainable production with the DEMATEL method, Int. J. Adv. Appl. Sci. 9 (2022) 116–125. https://doi.org/10.21833/ijaas.2022.10.015.

[7] M. Pagac, J. Hajnys, Q.P. Ma, L. Jancar, J. Jansa, P. Stefek, J. Mesicek, A review of vat photopolymerization technology: Materials, applications, challenges, and future trends of 3d printing, Polymers (Basel). 13 (2021) 1–20. https://doi.org/10.3390/polym13040598.

[8] C. Noè, A. Cosola, C. Tonda-Turo, R. Sesana, C. Delprete, A. Chiappone, M. Hakkarainen, M. Sangermano, DLP-printable fully biobased soybean oil composites, Polymer (Guildf). 247 (2022). https://doi.org/10.1016/j.polymer.2022.124779.

[9] C. Mendes-Felipe, I. Isusi, O. Gómez-Jiménez-Aberasturi, S. Prieto-Fernandez, L. Ruiz-Rubio, M. Sangermano, J.L. Vilas-Vilela, One-Step Method for Direct Acrylation of Vegetable Oils: A Biobased Material for 3D Printing, Polymers (Basel). 15 (2023). https://doi.org/10.3390/polym15143136.

[10] L.Y. Zhou, J. Fu, Y. He, A Review of 3D Printing Technologies for Soft Polymer Materials, Adv. Funct. Mater. 30 (2020) 1–38. https://doi.org/10.1002/adfm.202000187.

[11] A. Medellin, W. Du, G. Miao, J. Zou, Z. Pei, C. Ma, Vat photopolymerization 3d printing of nanocomposites: A literature review, J. Micro Nano-Manufacturing. 7 (2019). https://doi.org/10.1115/1.4044288.

[12] A. Barkane, O. Platnieks, M. Jurinovs, S. Kasetaite, J. Ostrauskaite, S. Gaidukovs, Y. Habibi, Uv-light curing of 3d printing inks from vegetable oils for stereolithography, Polymers (Basel). 13 (2021) 1–16. https://doi.org/10.3390/polym13081195.

[13] Z.S. Petrovic, Polyurethanes from vegetable oils, Polym. Rev. 48 (2008) 109–155. https://doi.org/10.1080/15583720701834224.

[14] L. Fertier, H. Koleilat, M. Stemmelen, O. Giani, C. Joly-Duhamel, V. Lapinte, J.J. Robin, The use of renewable feedstock in UV-curable materials-A new age for polymers and green chemistry, Prog. Polym. Sci. 38 (2013) 932–962. https://doi.org/10.1016/j.progpolymsci.2012.12.002.

[15] S. Zakeri, M. Vippola, E. Levänen, A comprehensive review of the photopolymerization of ceramic resins used in stereolithography, Addit. Manuf. 35 (2020) 101177. https://doi.org/10.1016/j.addma.2020.101177.

[16] C. Vazquez-Martel, L. Becker, W. V. Liebig, P. Elsner, E. Blasco, Vegetable Oils as Sustainable Inks for Additive Manufacturing: A Comparative Study, ACS Sustain. Chem. Eng. 9 (2021) 16840–16848. https://doi.org/10.1021/acssuschemeng.1c06784.

[17] V.S.D. Voet, J. Guit, K. Loos, Sustainable Photopolymers in 3D Printing: A Review on Biobased, Biodegradable, and Recyclable Alternatives, Macromol. Rapid Commun. 42 (2021) 1–11. https://doi.org/10.1002/marc.202000475.

[18] M. Lebedevaite, V. Talacka, J. Ostrauskaite, High biorenewable content acrylate photocurable resins for DLP 3D printing, J. Appl. Polym. Sci. 138 (2021). https://doi.org/10.1002/app.50233.

[19] S. Miao, W. Zhu, N.J. Castro, M. Nowicki, X. Zhou, H. Cui, J.P. Fisher, L.G. Zhang, 4D printing smart biomedical scaffolds with novel soybean oil epoxidized acrylate, Sci. Rep. 6 (2016) 1–10. https://doi.org/10.1038/srep27226.

[20] Z. Liu, D.A. Knetzer, J. Wang, F. Chu, C. Lu, P.D. Calvert, 3D printing acrylated epoxidized soybean oil reinforced with functionalized cellulose by UV curing, J. Appl. Polym. Sci. 139 (2022) 1–10. https://doi.org/10.1002/app.51561.

[21] Y. Zhang, Y. Li, V.K. Thakur, L. Wang, J. Gu, Z. Gao, B. Fan, Q. Wu, M.R. Kessler, Bio-based reactive diluents as sustainable replacements for styrene in MAESO resin, RSC Adv. 8 (2018) 13780–13788. https://doi.org/10.1039/c8ra00339d.

[22] Y. Zhang, Y. Li, L. Wang, Z. Gao, M.R. Kessler, Synthesis and Characterization of Methacrylated Eugenol as a Sustainable Reactive Diluent for a Maleinated Acrylated Epoxidized Soybean Oil Resin, ACS Sustain. Chem. Eng. 5 (2017) 8876–8883. https://doi.org/10.1021/acssuschemeng.7b01673.

[23] A. Cosola, M. Sangermano, D. Terenziani, R. Conti, M. Messori, H. Grützmacher, C.F. Pirri, A. Chiappone, DLP 3D – printing of shape memory polymers stabilized by thermoreversible hydrogen bonding interactions, Appl. Mater. Today. 23 (2021) 101060. https://doi.org/10.1016/j.apmt.2021.101060.

[24] C. Mendes-Felipe, R. Cofano, A. Garcia, M. Sangermano, S. Lanceros-Mendez, Photocurable 3D printed anisotropic electrically conductive materials based on bio-renewable composites, Addit. Manuf. 78 (2023) 103867. https://doi.org/10.1016/j.addma.2023.103867.

[25] K.G. McCurdy, K.J. Laidler, Rates of Polymerization of Acrylates and Methacrylates in Emulsion Systems, Can. J. Chem. 42 (1964) 825–829. https://doi.org/10.1139/v64-122.

[26] T.J. Hammer, H.M.S. Mehr, C. Pugh, M.D. Soucek, Urethane methacrylate reactive diluents for UV-curable polyester powder coatings, J. Coatings Technol. Res. 18 (2021) 333–348. https://doi.org/10.1007/s11998-020-00391-8.

[27] A.R. Jagtap, A. More, Developments in reactive diluents: a review, Springer Berlin Heidelberg, 2022. https://doi.org/10.1007/s00289-021-03808-5.

[28] J. Huang, P. Fu, W. Li, L. Xiao, J. Chen, X. Nie, Influence of crosslinking density on the mechanical and thermal properties of plant oil-based epoxy resin, RSC Adv. 12 (2022) 23048–23056. https://doi.org/10.1039/d2ra04206a.

[29] X. Xu, L. Chen, J. Guo, X. Cao, S. Wang, Synthesis and characteristics of tung oil-based acrylated-alkyd resin modified by isobornyl acrylate, RSC Adv. 7 (2017) 30439–30445. https://doi.org/10.1039/c7ra02189e.

[30] D.R.T. Roberts, S.J. Holder, Mechanochromic systems for the detection of stress, strain and deformation in polymeric materials, J. Mater. Chem. 21 (2011) 8256–8268. https://doi.org/10.1039/c0jm04237d.